Bio-Compatible Ceramics as Mimetic Material for Bone Tissue Substitution

Zdenek Strnad*, Jaroslav Šesták**

*Laboratory for Glass and Ceramics (LASAK), Papírenská 25, CZ-16000 Prague 6, Czech Republic
**Division of Solid-State Physics, Institute of Physics of the Czech Academy of Sciences, Cukrovarnická 10, CZ-16253 Prague 6, Czech Republic

ABSTRACT

Bone-like apatite formation on the surface of implant is of key importance during the physical and chemical processes leading to the formation of bonds between the implanted material and the newly formed bone tissue. The smartness of such a mimetic process is likely the action of silanole groups (Si-OH) which serve as the nucleation sites for the biocompatible interface formation capable to coexist between the original tissue and the implants which can be made from ceramics, glass-ceramics, composites as well as certain metals (titanium) respecting the condition of suitable surface reactivity. Lasak Co.Ltd., is the leading manufacturer of these materials in the Czech Republic and provides various kinds of bioactive implants, based on calcium phosphate ceramics, apatite wollastonite glass-ceramics and implants with hydroxyapatite surface coatings, permitting differentiated applications in clinical practice. The bioactive materials used as bone substitutes are all the subject of continuing research to attain biological, mechanical and chemical properties as similar as possible to those of the tissue to be replaced – mimetic materials. Clinical applications in orthopaedics, neurosurgery, maxillofacial surgery, auricular surgery, dental surgery and in other fields are demonstrated.

Keywords: biaoctive implants, bone substitutes, glass-ceramics, hydroxyapatite

INTRODUCTION

Degeneration of the skeletal system in time results in dysfunction of bones, teeth and joints. Extensive bone defects left after the removal of tumours, infections or as a result of injuries are ideally replaced by autogenic bone tissue. As the amount of this material for the patient is limited and the use of allogenic bone is accompanied by biological, mechanical and also sociological difficulties, there is a great need for alternate material.

Since discovery of Bioglass in 1971 (1), various kinds of bioactive materials have been found and clinically used. The uniqueness of surface bioactive materials is their high bioactivity, opening qualitatively new application fields, especially for anchoring of the implant in the host tissue, with practical use in orthopedics, stomatology, neurosurgery, oncology, craniofacial surgery and possibly other fields.

LASAK developed and provides three basic kinds of bioactive materials, BAS-O, BAS-HA and BAS-R, permitting differentiated applications in clinical practice. More than 7000 people received these implants as their bone substitutes during last eight years.

BAS-O GLASS-CERAMICS - BIOACTIVE LONG-TERM STABLE IMPLANT MATERIAL WITH HIGH MECHANICAL STRENGTH

BAS-O is an inorganic, polycrystalline material prepared by controlled crystallization of glass, whose main components are CaO, P205, Si02 MgO, and Al2O3 During the crystallization process, the amorphous material is converted to a glass-ceramic material whose main crystalline phases are apatite and wollastonite (2,3). Controlled crystallization permits not only controlled phase conversion during the process, but also

control of the chemical composition and structure of the residual glass phase, which are decisive factors in determining the bioactivity of the final material (4).

BAS-O exhibits extraordinary biocompatibility, which has been demonstrated in many experiments and clinical tests. The basic condition for the formation of a bond between the BAS-O implant and the living bone tissue is the formation of a thin layer enriched in Ca and P on the glass-ceramic surface as a result of a reaction between the implant and body fluids (Fig,1).

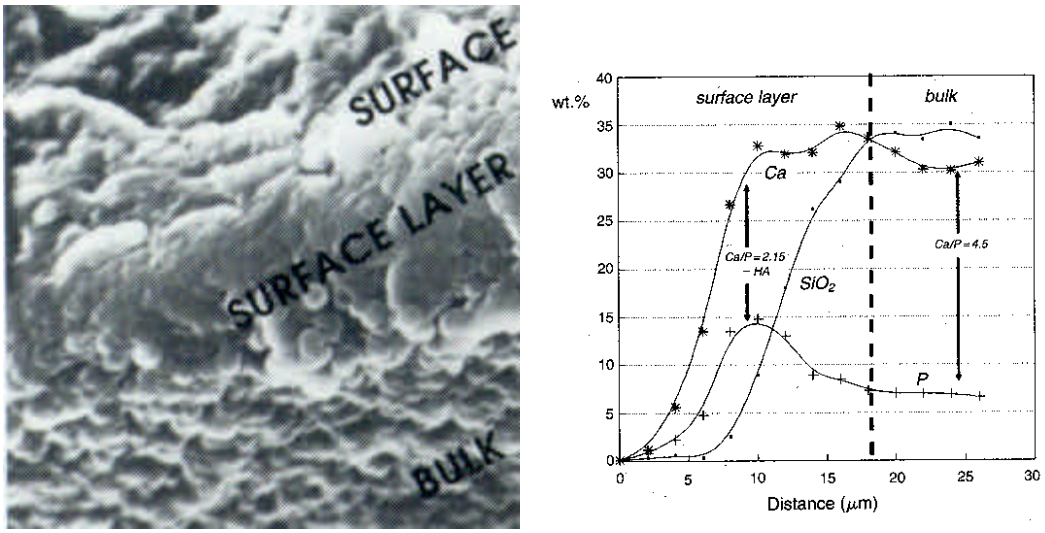

a. **b.**

Fig. 1. Surface layer formed on a BAS-O implant after exposure in a simulated body fluid for 28 days**.**
a. Cross-section through the surface layer (SEM 1000x),
b. Content of elements (P, Ca and SiO2) in the surface layer.

This layer, which is initially amorphous, changes in time to form a polycrystalline layer of apatite agglomerates, into which are incorporated organic components in the interface zone, produced by osteoblasts, such as collagen fibers, with the formation of a tight bond (Fig. 2).

Fig.2: Detail of the interface of the bone tissue with a BAS-O implant 6 months after implantation (SEM).

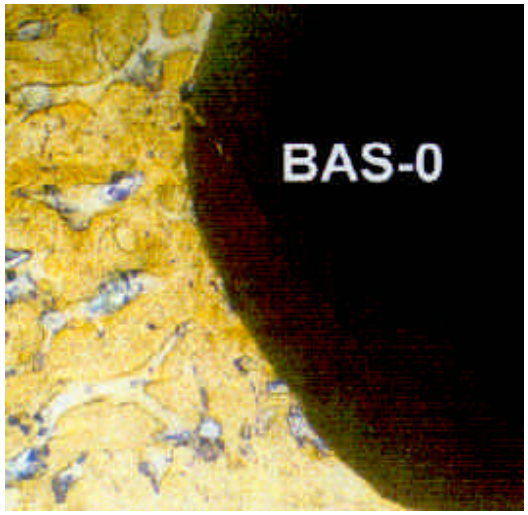

Fig.3: Photomicrograph of a section of BAS-0 granule implant in bone, 2 years after implantation (toluidine blue stain).

Thus, the implant is not considered to be a foreign body; on the contrary, a strong bond is formed directly between the implant and the bone tissue, without an intermediate layer of soft tissue, in a time period of 4-8 weeks after implantation (Fig. 3).

BAS-O exhibits intense osteoconductive properties and also the ability to form bonds between the individual BAS-O particles in a body fluid medium. BAS-O is a white material with an apparent density of 3000-3100 kg/m3. The material has a similar bending strength to the cortical bone, 170 MPA, and approximately double the compressive strength, > 400 MPa. The strength of the junction of the BAS-O implant with bone tissue, measured by the push-out test (with shear stress) after implantation for 2 months is 15-20 MPa.

Clinical application

BAS-0 granules and ground material are used to fill cysts, defects left by injuries, defects left by excochleation of benign tumors, and to reconstruct extensive acetabular defects (Fig. 4). Compact, wedge-shaped blocks (with various heights and surfaces) can be used, e.g., for condyl elevation. Individually shaped implants can be used in neurosurgery to cover defects left from cranial trepanation and as onlays in plastic surgery.

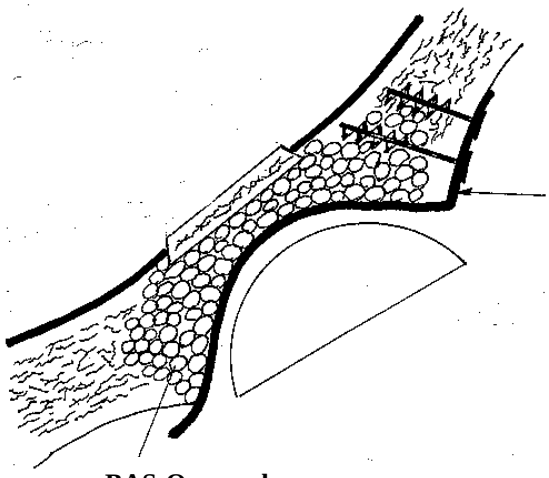

a. **b.**

Fig. 4: Reconstruction of extensive acetabular defects by bioactive glass-ceramics BAS-0 in reoperation of total endoprotheses. **a.** Schematic drawing of implantation. **b.** Radiogram taken 8 months post-operatively. [5]

The special shape of intervertebral prostheses have been developed and successfully used in surgery of spin (Fig. 5). In cranio-facial surgery, the material can be used as plates, blocks, or individually shaped implants to replace bone defects, rebuilding of orbit, for reconstruction of partial mandibular defects. It can be used to enlarge the mandible or for plastic chin and nose profiles.

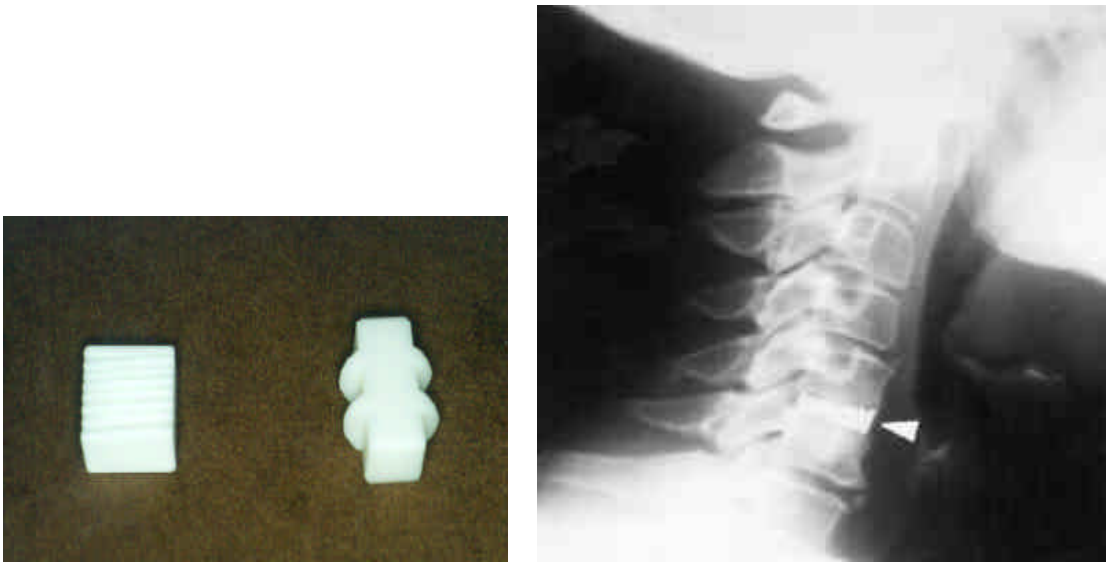

a. **b.**

Fig.5: **a.** BAS-0 intervertebral prostheses. **b.** Radiogram taken post-operatively [6].

BAS-HA - BIOACTIVE NONRESORBABLE IMPLANT MATERIAL BASED ON HYDROXYAPATITE $CA_{10}(P0_4)_6(OH)_2$

Hydroxyapatite is synthesized from aqueous solutions under precisely defined pH, temperature and other physical parameters, which ensure reproducible preparation of a highly pure, crystallographically defined product, which does not contain any unwanted calcium phosphates. This product is further processed to yield the final BAS-HA product with defined biophysical properties., Its structure and composition are similar to bio-apatite, which is the main inorganic component of living bone tissue. Implants form a strong: bond between the bone tissue and the implant material without an intermediate fibrous layer (Fig. 6).

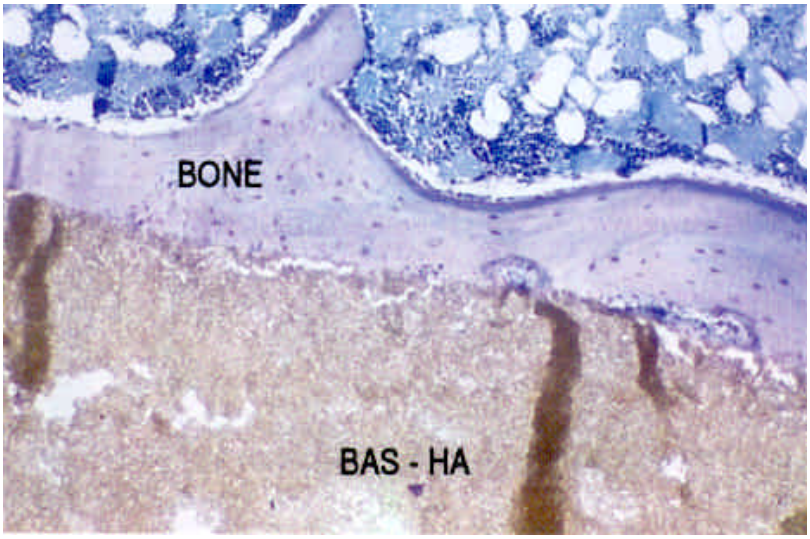

Fig.6: Direct contact between the BAS-HA implant and bone tissue, 2 months after implantation (thin-section, toluidine blue stain)

BAS-HA exhibits high biocompatibility, which has been demonstrated in many preclinical and clinical tests, including tests of cytotoxicity, carcinogenesis and mutagenic effects. The material exhibits osteoconductive properties. After implantation in the defective part of the bone, bone tissue is newly

formed in the space between the granules of this substance. A complex of artificial substances and living bone tissue is formed.

BAS-HA is a very dense ceramic with apparent porosity of 1.7 %. The Ca/P molar ratio is 1.66. The material exhibits a bending strength of 60 MPa and compression strength of 200 MPa. The strength of the junction with the bone tissue measured by the push-out test (shear stress) is equal to 19 MPa two months after implantation and 29 MPa 4 months after implantation.

Clinical application

BAS-HA material is designed for bone grafting especially at sites where only compressive forces are expected to act on the implant. It can be used in dentoalveolar surgery to fill bone defects left after extirpation of cysts, surgical extractions, or to remodel the alveolar ridge. In paradontology, it can be used to treat bone paradontological defects. Bioactive BAS-HA material is also used for production of middle ear implants (Fig. 7) and dental implants with hydroxyapatite coating (Fig. 8) [7, 8].

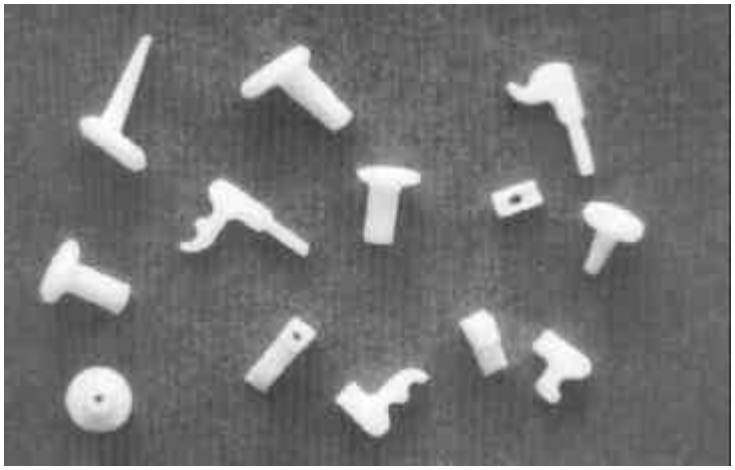

Fig.7: Middle ear implants made of BAS-HA.

Fig.8: Dental implant (Impladent) with hydroxyapatite coating.

BAS-R - BIOACTIVE RESORBABLE IMPLANT MATERIAL BASED ON TRICALCIUM PHOSPHATE $CA_3(P0_4)_2$

BAS-R is a surface bioactive, resorbable, inorganic, crystalline material based on tricalcium phosphate (β-TCP) .The material is prepared by a special procedure at high temperature by melting and controlled cooling of the melt. BAS-R forms direct bonds with living bone tissue without forming a fibrous interlayer.

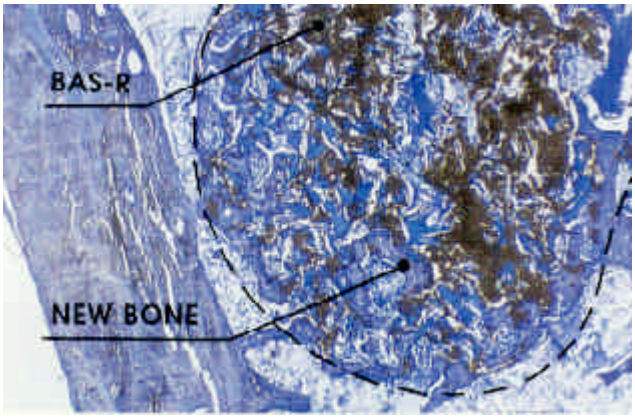

Fig. 9. Gradual resorption of granules (- - -) of BAS-R and simultaneous formation of new bone tissue at the edges of the granules; 8 months after implantation (thin-section, toluidine blue stain)

The material greatly stimulates formation of new bone tissue and has osteoconductive properties. The material gradually disintegrates in the body as .a consequence of hydrolytic corrosion and active phagocytosis, accompanied by resorption and replacement with newly formed bone tissue (Fig. 9) BAS-R is white in color and has an apparent density of 2900-3100 kg/m3

Clinical application

It is designed for bone replacement where resorption is required, with gradual replacement by living bone tissue. It is used in paradentology and in dentoalveolar surgery to treat bone defects [10] (see Fig.10).

Fig.10: Filling of bone defects left by tooth extraction and extirpation of a radicular cyst a) prior to the operation b) after application of BAS-R

OUTLOOK

Today bioceramics are used in a broad field of devices inside the human body. This is mainly due to their good biocompatibility. Among the ceramic materials used for bone replacement, bioactive ceramics appear particularly promising because of their ability to form stable interface with living host tissue. The major problem of these materials, which inhibits their application on several types of implants, is their poor match of mechanical behavior of the implant with the tissue to be replaced. Principally, the coating, composites, porous structured materials and/or new resorbable materials are promising ways for the next development.

However, no one has succeeded todate, in finding a material, which fully corresponds to bone or other living parts of the body. It is the task of a growing number of researchers and institutions working in the field of biomaterials to further improve performance of these materials. Nature is still the better engineer.

REFERENCES

1. L.L.Hench, R.S.Splinter, W.S.Allen, 1971. Bonding mechanisms at the interface of ceramic prosthetic materials, J.Biomed,Res.Symp. 2, 117.
2. Z.Strnad, 1986. Glass-Ceramic Materials/Liquid Phase Separation, Nucleation and Crystallization in Glasses, Elsevier, Amsterdam.
3. Z.Strnad, K.Urban, 1989. Surface Bioactive Glass-Ceramic Materials, Sklár a keramik, 39, 292.
4. Z.Strnad, 1992. Role of the Glass Phase in Bioactive glass-ceramics, Biomaterials, 13(5), 317.
5. K.Urban, P.Šponer, 1998. Reconstruction of Extensive Acetabular Defects by Bioactive Glass Ceramics in Re-operations of Total Endoprostheses, Acta Chir.Orthop.Traum.Cech., 65, 17.
6. M.Filip, P.Veselský, Z.Strnad, P.Laník, 1995. The Replacement of the Intervertebral Disc by Ceramic Prosthesis in Treatment of Degenerative Diseases of the Spine, Acta Chir.Ortho.Traum. Cech., 62, 226.
7. A. Šimunek, A. Štepánek, V.Zábrodský, Z.Nathanský, Z.Strnad, 1997. A 3-year Multicenter Study on Osseointegrated Implants- Impladent, Quintessenz 6(3).
8. Z.Strnad, J. Strnad, M.Psotová, C.Povýšil, K. Urban, 1998. The Osseoconductive Ability of Plasmatically Deposited Hydroxyapatite and Pure Ti in Vitro and in Vivo, Quintessenz, 7, 5.
9. K.Urban, Z.Strnad, C.Povýšil, P.Šponer, 1996. Tricalcium phosphate as a bone tissue substitute, Acta Chir.Orthop.Traum.Cech, 63, 16.
10. V.Pávek, Z.Novák, Z.Strnad, D.Kudrnová, 1994. Clinical Applications of Bioactive Glass-ceramics BAS-O for Filling Cyst Cavities in Stomatology, Biomaterials, 15(5), 353.

Yariv04

Journal of Thermal Analysis and Calorimetry, Vol. 71 (2003)

THERMODYNAMICS OF NON-BRIDGING OXYGEN IN SILICA BIO-COMPATIBLE GLASS-CERAMICS
Mimetic material for the bone tissue substitution

N. Koga[1], *Z. Strnad*[2], *J. Šesták*[3]* *and J. Strnad*[2]

[1]Chemistry Laboratory, Department of Science Education, Graduate School of Education, Hiroshima University, 1-1-1 Kagamiyama, Higashi-Hiroshima 739-8524, Japan
[2]Laboratory for Glass and Ceramics (LASAK), Papírenská 25, CZ-16000 Praha 6, Czech Republic
[3]Institute of Physics of the Academy of Sciences, Cukrovarnicka 10, CZ-16253 Praha and Institute of Interdisciplinary Studies, te West Bohemian University, Husova 17, CZ-30114 Pilsen, Czech Republic

Abstract

Correlations between the structural properties of Na_2O–CaO–SiO_2 glasses characterized by the activity of oxygen ions and the bioactivity were examined by comparing the compositional dependence of the structural parameters calculated on the basis of a thermodynamic consideration with that of the bioactivity. A simple model of characterizing the glass structure by considering the bridging and non-bridging oxygen ions was employed as the first step for this purpose. Further detailed thermodynamic analysis on the anionic constitution in the glass was performed and the compositional dependences of the relative proportions of bridging, non-bridging and free oxygen ions were calculated. The bioactive region corresponded to the compositional region characterized by the higher relative proportion of non-bridging oxygen ions with co-existing an appreciable concentration of bridging oxygen ions, suggesting a possible important role of the non-bridging oxygen ions on the surface chemical process of bone-like apatite layer formation.

Kevwords: bio-compatible, bone-like apatite, glass-ceramics, mimetic material, thermodynamics

Introduction

Degeneration of a human skeletal system in time results in dysfunction of bones, teeth and joints. Extensive bone defects, left after the removal of tumors, infections or as a result of injuries, are ideally replaced by autogenous bone tissue. As the amount of this material for the patient is limited and the use of allogenic bone is accompanied by biological, mechanical and also sociological difficulties, there is a great need for alternate non-human synthetic sources.

Merely four decades ago it was considered inconceivable that a man-made material could bond to living tissues in view of the deep-rooted experience that it would result in a

* Author for correspondence: E-mail: sestak@fzu.cz

1418–2874/2003/ $ 20.00
Akadémiai Kiadó, Budapest

foreign body reaction and the formation of non-adherent scar tissue at the interface with inserted material. This understanding was irreversibly altered when a special composition of soda-lime-phosphate-silica glass was synthesized by Hench [1] and successfully implanted in the femurs of rats. About 6% of P_2O_5 was added to simulate the Ca/P constituents of hydroxyapatite, $Ca_{10}(PO_4)_6(OH)_2$, that is the inorganic mineral phase naturally existing in bones. Therefore the bone-like apatite formation on the surface of implant is of a key importance during the physical and chemical processes leading to the formation of an enough firm connection between the implanted material and the newly formed bone tissue [2–6]. The bioactivity leads to both the osteoconduction and osteoproduction as a consequence of rapid reaction on the bioactive glass surface. The surface reactions [7–16] involve ionic dissolution of calcium and sodium ions, phosphates and hydrated silica that give rise to both the intercellular and extracellular responses at the interfaces of the glass with its physiological environment. The smartness of such a mimetic process is likely hidden in the activity of oxygen characterized by the action of silanole groups (Si–OH). They likely serve as the nucleation sites for the bio-compatible interface formation capable to coexist between the original tissue and the implants which can be expediently made from glass, glass-ceramics, ceramics, cements and other composites as well as from certainly treated metals (etched titanium) respecting the set-in condition of its suitable surface reactivity.

We have taken part in the research progress of bioactive materials since early eighties [17–22]. This matured in their actual appliance in practical implantology under the trademark IMPLADENT- (a system for oral implantology produced by LASAK, Co.

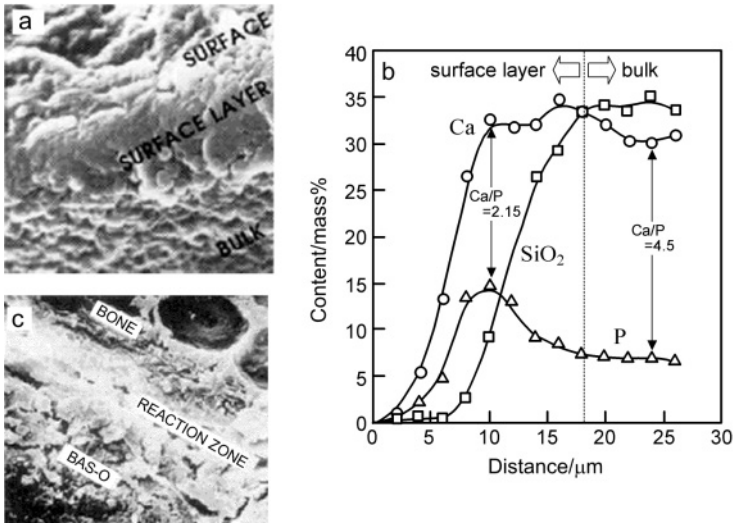

Fig. 1 Surface layer formed on a BAS-O implant after exposure in a simulated body fluid for 28 days (a) and the cross section of the actual body implant (c): a – View of the surface layer formed on the BAS-O material after exposure in SBF (SEM 1000×, fracture), b – Content of elements (P, Ca and SiO_2) in the surface layer, and c – Detail of the interface of the bone tissue with a BAS-O implant 6 months after implantation (SEM 1200×)

Ltd) and BAS-O, BAS-HA, BAS-R-bioactive bone tissue substitutes [23]. Figure 1 illustrates the bone-bonding ability of BAS-O which is based on inorganic, polycrystalline material prepared by controlled crystallization of glass, whose main components are CaO, P_2O_5, SiO_2 and MgO. During the crystallization process, the glassy material is converted to a glass-ceramic material whose main crystalline phases are apatite and wollastonite. BAS-O granules and ground material are used to fill cysts, defects left by injuries, defects left by excochleation of benign tumors, and can be of help to reconstruct extensive acetabular defects. Compact, wedge-shaped blocks (with various heights and surfaces) became useful for, e.g., condyl elevation. Individually shaped implants can be used in neurosurgery to cover defects left from cranial trepanation and as onlays in plastic surgery. In Fig. 2, there is revealed another case of biomaterial BAS-HA (hydroxyapatite) which is synthesized from aqueous solutions under precisely defined pH, temperature and other physical parameters, which ensure reproducible preparation of a highly pure, crystallographically defined product, which does not contain any unwanted calcium phosphates. Its structure and composition are similar to bio-apatite, which is the main inorganic component of living bone tissue. Implants form a strong bond between the bone tissue and the implant material without any intermediate fibrous layer. Final product is the BAS-R, which is the surface bioactive, resorbable, inorganic, crystalline material based on tricalcium phosphate.

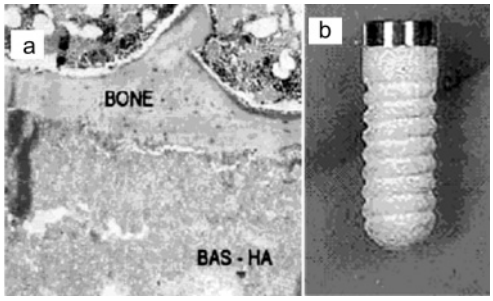

Fig. 2 a – Direct contact between the BAS-HA implant and bone tissue, 2 months after implantation. BAS-HA material is a very dense ceramics with apparent porosity of 1.7%. The Ca/P molar ratio is 1.66. The material exhibits a bending strength of 60 MPa and compression strength of 200 MPa. The strength of the junction with the bone tissue measured by the push-out test (shear stress) is equal to 19 MPa (two months after implantation) and 29 MPa (4 months after implantation).
b – Dental implant ('Impladent') with hydroxyapatite coating

Bioactivity has since attracted increased attention being aimed to further molecular manipulation (doping surfactants, micro-additives of various organic molecules such as proteins, glyco-proteins and polysaccharides, useful in easier mine-realization) which intelligent response by host organism is evaluated in order to achieve well-tailored implants. Bio-glass-ceramics that activate genes offer the possibilities of repairing, or perhaps even preventing, many disease states, such as osteoporosis, in which a large fraction of women lose a substantial amount of bone mass as they age. They can be also used as a second phase in a composite that mimics the structure and properties of bone. In future

the implication of glass activation of genes it may be possible to design therapeutic treatments or food additives that will inhibit the deterioration of connective tissues with age. Further understanding bioactivity may even help in better perception of the creation of life [24–26]. It shows a great variability in the application of different glasses and amorphous materials in many fields of human activities [23, 27–31].

Structural parameters of the soda-lime-silica glasses and bioactivity

It is generally accepted that the bioactivity of glass and glass-ceramics is closely connected with the surface chemical reactions of formation of a bone-like apatite layer that bonds to the bone [2–6]. Very important is systematic understanding on mechanisms and kinetics of the reactions that occur at the surface of glassy implants of silica-specialized composition. The early stages of the bone-like apatite formation on a surface of bioactive glass have been studied systematically [7–16] and summarized as follows [16]. The alkali ions in the bioactive glass are rapidly exchanged by hydrogen ions in the surrounding solution, e.g., body or simulated body fluids (SBF), and the network dissolution rapidly reduce the amount of the Si–O–Si and Si–O–Ca modes and replace them with Si–OH bonds at the glass-solution interface. Single non-bridging oxygen modes of Si–OH are then gradually replaced by more spherical OH–Si–OH and the condensation and repolymerization of a SiO_2-rich layer take place on the surface. An amorphous $CaO–P_2O_5$-rich film is produced on the top of the SiO_2-rich layer by incorporating soluble calcium and phosphate from solution. The characteristic double layer composed of a SiO_2-rich layer and a mixed crystalline layer of hydroxy carbonate apatite and/or hydroxyl fluorapatite results from the crystallization of the amorphous $CaO–P_2O_5$-rich film by incorporating OH^-, CO_3^{2-}, or F^- anions from the surrounding solution.

The rates of consecutive and/or concurrent chemical processes of bone-like apatite formation on the glass surface depend largely on the composition of glass or glass-ceramics and on the associated physico-chemical properties of these materials such as solubility, volumetric ratios of glass phase and so on [7–16]. An evaluation of the correlation of the bioactivity with the structure of glasses is thus of interest, as have been the cases of the compositional dependence of all physico-chemical properties of glass, such as viscosity, electrical properties, immiscibility, glass formation region, nucleation, crystallization, phase separation, and so on [23, 27, 28, 32–40]. The constitution of bridging and non-bridging oxygen ions in glasses [23] is one of the most frequently used concept for characterizing the glass structure. Various physico-chemical properties have been correlated to the chemical composition in view of the thermodynamic state of oxygen ions. Although there are various different theories on evaluating the constitution of bridging and non-bridging oxygen ions in glasses [41–45], earlier we evaluated the state of oxygen ions in an iron-rich borate glasses [46] according to the model proposed by Toop and Samis [42]. In the present case of bioactivity, the state of oxygen ions is also likely important in relation to the chemical processes of the early stage of the bone-like apatite

formation, especially in the dissolution process of Si–O–Si mode with bridging oxygen and intermediate formation of Si–OH with non-bridging oxygen. Previously, one of the present authors was evaluated the correlation of the bioactivity of Na_2O–CaO–SiO_2–P_2O_5 and CaO–MgO–SiO_2–P_2O_5 glass-ceramic systems with the structural parameter related to the bridging oxygen [17] using the Stevels model [41].

The Stevels's parameters [17, 41], i.e., *X* and *Y*, can be correlated to the mean number of non-bridging (O^-) and bridging (O^o) oxygen ions per polyhedron in the glass lattice, respectively, and calculated from the molar composition of glass according to the following equations.

$$X=2R-Z$$

$$Y=2Z-2R$$

where *Z* is the mean number of all types of oxygen ions per polyhedron, i.e., the mean coordination number of the glass-forming cations and *R* is the ratio of the total number of oxygen ions to the total number of glass-forming cations in glass. The parameters (*X*, *Y*) vary from (0, 4) for, e.g., the pure silica glass, to (1, 3) for, e.g., $Na_2O{\cdot}2SiO_2$ glass, and to (2, 2) for, e.g., $CaO{\cdot}Na_2O{\cdot}2SiO_2$ glass. When $X>2$ and $Y<2$, the glasses are called as invert glasses. Having the same values of (*X*, *Y*), these glasses are characterized as structurally similar.

In the previous work on the Na_2O–CaO–SiO_2–P_2O_5 and CaO–MgO–SiO_2–P_2O_5 glass-ceramic systems [17], the bioactivities of these systems evaluated by in vitro test of mutual bonding after soaking in SBF and by in vivo test of implantation in dog tibia were correlated to one of the Stevels's parameter *Y*, i.e., mean number of bridging oxygen ions. It was found that the *Y* value of the residual glass phase in the glass-ceramic system to be close to 2 is the suitable condition for the higher bioactivity. When $Y>3$, the glass loses its bioactivity.

In the present study, the attention was turned to the non-bridging oxygen ions in the glass as expressed by the Stevels's parameter *X*. In order to correlate the structural parameter *X* of a glass with its bioactivity, we focused on an empirical index of bioactivity,

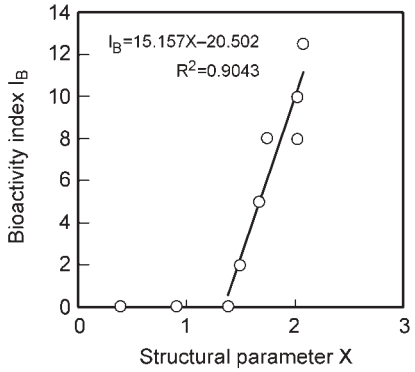

Fig. 3 Bioactive index I_B as a function of mean number of non-bridging oxygen ions *X*, calculated using the data of compositional dependence of I_B in the soda-lime--silica system containing 6 mass% P_2O_5 reported by Hench [2, 16, 47, 48]

I_B, introduced by Hench [47] as $I_B=100/t_{0.5bb}$, where $t_{0.5bb}$ is the time for more than 50% of the implant interface to be bonded to bone. The compositional dependence of I_B in the Na_2O–CaO–SiO_2 system containing 6 mass% P_2O_5 has been clearly represented by Hench [2, 16, 47, 48] and employed usefully to discuss the bioactivity of the glass with a certain composition. By reading the values of I_B at various typical points of glass composition from the reported Iso I_B plots in the Na_2O–CaO–SiO_2 ternary system [2, 16, 47, 48], we calculated the structural parameters (X, Y) from the molar composition and relations of these structural parameters and the value of I_B were examined. Figure 3 shows the correlation between the calculated structural parameter X and the value of I_B for the Na_2O–CaO–SiO_2 ternary system containing 6 mass% P_2O_5. When X<1.5 (Y>2.5), the glass looses its bioactivity and bioactivity index, I_B~0. The value of X>1.5 (and Y<2.5) indicates the range of bioactive glasses, I_B>0. Essentially a linear dependence with negative intercept has been found between the mean number of non-bridging oxygen ions and bioactivity index.

Anionic constitution in the soda-lime-silica glass-forming melts and bioactivity

Since the Stevels model considers only non-bridging and bridging oxygen ions, it cannot hold in the more basic regime (X>>2) where free oxygen ions reach an appreciable concentration. Therefore, after Fincham and Richardson [49], one can propose the dominant reaction in the formation of silicate solution (glass): $O^o+O^{2-}=2O^-$ where O^{2-} refers to the free oxygen ions. The compositional dependence of relative proportion of non-bridging oxygen ions [O^-] in the soda-lime-silica system has been also calculated applying methods currently used in the chemistry of organic polymers.

According to Masson [43–45], the following assumptions were applied to derive the anionic distribution in M_2O–SiO_2 or MO–SiO_2 glass forming melts:

1) The silicate ions are presented exclusively as linear and branched chains of general formula: $Si_xO_{3x+1}^{(2x+2)-}$. These species may arise by the poly-condensation reactions expressed generally according to the following equation:

$$Si_xO_{3x+1}^{(2x+2)-}+Si_yO_{3y+1}^{(2y+2)-}=Si_{x+y}O_{3(x+y)+1}^{(2x+2y+2)-}+O^{2-} \quad (1)$$

2) The equilibrium constant k_{xy} of Eq. (1) can be approximated using that for the lowest k-members k_{11}, i.e., x=1 and y=1.

3) The Eq. (1) may be written in a more general form:

$$2O^-=O^o+O^{2-} \quad (2)$$

where O^-, O^o and O^{2-} are the non-bridging oxygen, bridging oxygen and free oxygen ions, respectively.

4) According to the Temkin's equation [50], the activity of M_2O or MO oxides in the M_2O–SiO_2 or MO–SiO_2 binary melt a_{MO} is equated to the ion fraction of free oxide ion $N_{O^{2-}}$.

$$a_{MO} = N_{O^{2-}} \tag{3}$$

5) For linear and branched chains, the a_{MO} has the following relation with respect to the mole fraction of SiO_2, i.e., for X_{SiO_2} it follows

$$\frac{1}{X_{SiO_2}} = 2 + \frac{1}{1 - a_{MO}} - \frac{3}{1 + a_{MO}\left(\frac{3}{k_{11}} - 1\right)} \tag{4}$$

6) Knowing the value of k_{11} for the binary system M_2O–SiO_2 or MO–SiO_2, the ion fraction N_x of any silicate ion $Si_xO_{3x+1}^{(2x+2)-}$ is given by the following equation:

$$N_x = \frac{(3x)!}{(2x+1)!x!}\left[\frac{1}{1+\frac{3a_{MO}}{k_{11}(1-a_{MO})}}\right]^{x-1}\left[\frac{1}{1+\frac{k_{11}(1-a_{MO})}{3a_{MO}}}\right]^{2x+1}(1-a_{MO}) \tag{5}$$

7) The ion fraction of non-bridging oxide N_{O^-} in Eq. (2) is approximated by the summation of N_x using x up to 50.

$$N_{O^-} = \sum_{x=1}^{50} N_x \tag{6}$$

8) The ion fraction of bridging oxide N_{O^o} is then obtained by

$$N_{O^o} = 1 - N_{O^{2-}} - N_{O^-} \tag{7}$$

Taking the literature values for $k_{11}=1.6\cdot10^{-3}$ and $=8\cdot10^{-8}$ for CaO–SiO_2 and Na_2O–SiO_2 binary melts [51], respectively, the X_{SiO_2} dependence of a_{MO} can be calculated according to Eq. (4). Figure 4 shows the compositional dependence of a_{MO} for CaO–SiO_2 and Na_2O–SiO_2 systems. The ion fraction N_x is obtained according to Eq. (5). The calculated ion fractions N_x for CaO–SiO_2 and Na_2O–SiO_2 binary melts are represented in Fig. 5 as a function of mass fraction of SiO_2. Using the compositional dependences of the activity of oxides, i.e., $N_{O^{2-}}$, shown in Fig. 4 and the relative propor-

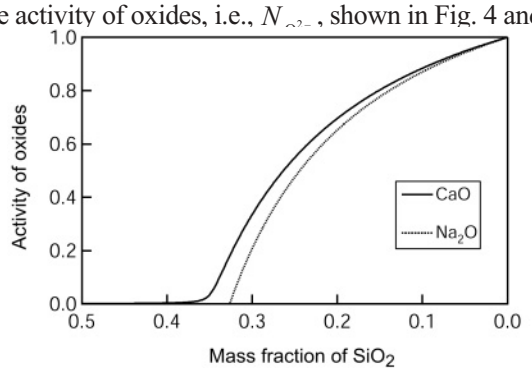

Fig. 4 The dependence of activity of sodium and calcium oxides, a_{MO}, on the mass fraction of SiO_2 in the binary CaO-SiO_2 and Na_2O-SiO_2 systems

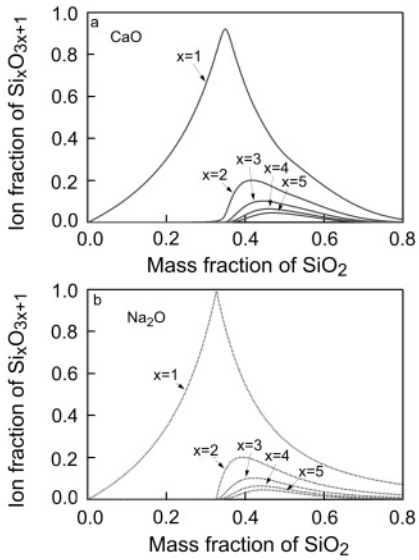

Fig. 5 The dependence of ion fraction N_x of silicate ions $Si_xO_{3x+1}^{(2x+2)-}$ on the mass of SiO_2 in the binary a – $CaO–SiO_2$ and b – $Na_2O–SiO_2$ systems

tions of O^- obtained by summing up N_x from x=1 to 50, the relative fraction of bridging oxygen ions N_{O^o} at a mass fraction of SiO_2 was calculated according to Eq. (7). Figure 6 shows the compositional dependences of the relative fractions of O^o, O^- and O^{2-} in the binary $CaO–SiO_2$ and $Na_2O–SiO_2$ systems. According to the conventional pseudo-binary assumption [52], the compositional dependence of the relative proportion of O^- in $Na_2O–CaO–SiO_2$ ternary melts was obtained using the values for the binary melts shown in Fig. 6. The compositional dependence (in mass fraction) of the calculated relative proportion of O^- in the $Na_2O–CaO–SiO_2$ ternary melts is shown in Fig. 7. These findings were compared with the compositional dependence of I_B for the system containing

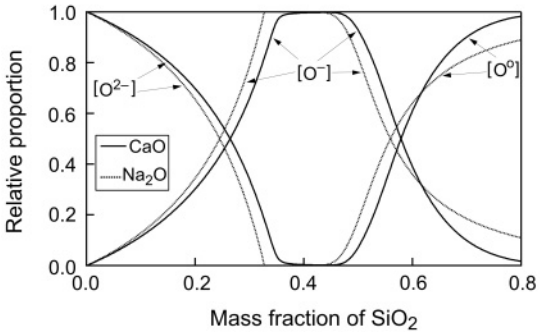

Fig. 6 The relative proportions of non-bridging oxygen ions O^-, bridging oxygen ions O^o and free oxygen ions O^{2-} in the binary a – $CaO–SiO_2$ and b – $Na_2O–SiO_2$ systems, calculated *vs*. the mass fraction of SiO_2 using the relations in Eqs (3), (6) and (7)

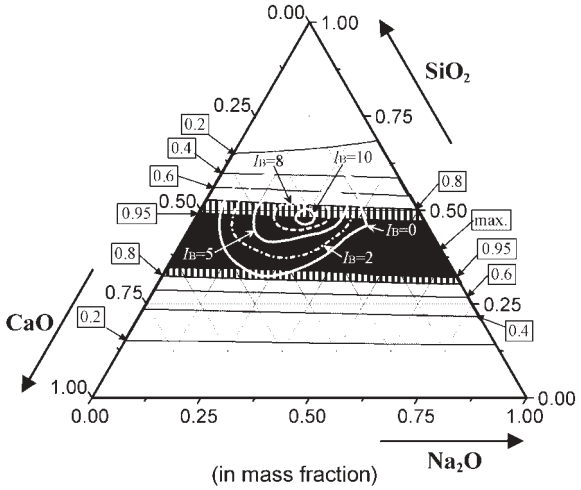

Fig. 7 A comparison of the relative proportion of non-bridging oxygen ions O^- in the Na_2O–CaO–SiO_2 ternary system calculated in the present study with the Iso I_B plots for the system with 6 mass% P_2O_5 reported by Hench [2, 16, 47, 48]

6 mass% P_2O_5 [2, 16, 47, 48]. The region of the remarkable high bioactivity I_B>8 can be observed in the compositional region characterized by the higher relative proportion of non-bridging oxygen ions >0.8 in the side of SiO_2-rich composition where an appreciable concentration of bridging oxygen ions exist, Fig. 7.

The ability to form the bone-like apatite layer after soaking P_2O_5-free Na_2O–CaO–SiO_2 glasses in SBF has been investigated experimentally by Kim *et al*. [53]. It was shown that the compositional region of the apatite layer formation on the surface of the P_2O_5-free Na_2O–CaO–SiO_2 glasses corresponds closely to the region of I_B>0 for the Na_2O–CaO–SiO_2 glasses containing 6 mass% P_2O_5. It was also pointed out that the rates of apatite formation of P_2O_5-containing Bioglass 45S5-type and a corresponding P_2O_5-free Na_2O–CaO–SiO_2 glass are comparable. Those findings indicate that the bioactivity of the glass characterized by the bone-like apatite formation depends largely on the properties of the basic P_2O_5-free Na_2O–CaO–SiO_2 ternary glass. From the present results, it is predicted that a close connection exists between the structural property of the glass characterized by the activity of oxygen ions and its bioactivity. The special notice is concerning the proportion of non-bridging oxygen ions in the glasses, where the region of remarkable high bioactivity is observed for the compositional region with the higher relative proportion of non-bridging oxygen ions >0.8, indicating a possible important role of the non-bridging oxygen ions during the course of the surface chemical processes of bone-like apatite layer formation.

Conclusions

A close correlation between the structural properties of the Na_2O–CaO–SiO_2 glasses and its bioactivity was found. Using the structural parameters X and Y related, respectively, to the mean number of non-bridging and bridging oxygen ions, the bioactive region can be correlated to the structural parameters $X>1.5$ and $Y<2.5$. Further detailed analysis of the anionic constitution in the glass system indicated that the remarkable high bioactive region is seen in the compositional region of higher relative proportion of non-bridging oxygen ions with co-existing an appreciable concentration of bridging oxygen ions and no significant free oxygen ions.

The structural correlations of the bioactivity shown in the present study can be used as a useful tool for designing the bioactive glass and for tailoring bioactive glass-ceramics and composites with a glass-ceramic matrix. At the same time, a possible important role of the non-bridging oxygen ions on the surface chemical processes of the bone-like apatite layer formation is expected from the close correlation of the relative proportion with the bioactivity.

* * *

The authors express thanks and gratitude to the Grant Agency of the Academy of Sciences of the Czech Republic for the project financing. The grant A 4010101 is especially acknowledged as well as the project support by the dept. of industry of the Czech Republic under the number: FB-CV/64.

References

1 L. L. Hench, R. J. Splitner, W. C. Allen and T. K. Greenlee, J. Biomed. Mater. Res., 2 (1971) 117.
2 L. L. Hench, J. Am. Ceram. Soc., 74 (1991) 1487.
3 T. Kokubo, Biomater., 12 (1991) 155.
4 L. L. Hench and J. Wilson, Introduction to Bioceramics, World Sci. Publ., London 1993.
5 L. L. Hench and J. K. West, Life chemistry reports, 13 (1996) 187.
6 L. L. Hench, J. Am. Ceram. Soc., 81 (1998) 1705.
7 L. L. Hench and H. A. Paschal, J. Biomed. Mater. Res., 4 (1973) 25; 5 (1974) 49.
8 T. Kokubo, S. Ito, S. Sakka and T. Yamamuro, J. Mater. Sci., 20 (1985) 2001; 21 (1986) 536.
9 W. Holand, W. Vogel, K. Neumann and J. Gummel, J. Biomed. Mater. Res., 19 (1985) 303.
10 A. E. Clark and L. L. Hench, J. Non-Cryst. Solids, 113 (1989) 195.
11 L. L. Hench and J. K. West, Chem. Rev., 90 (1990) 33.
12 T. Kokubo, J. Non-Cryst. Solids, 120 (1990) 138.
13 O. H. Andersson, K. H. Karlsson and K. Kangasniemi, J. Non-Cryst. Solids, 119 (1990) 290.
14 T. Kokubo, Thermochim. Acta, 280/281 (1996) 479.
15 W. Cao and L. L. Hench, Ceramics Int., 22 (1996) 493.
16 O. Peitl, E. D. Zanotto and L. L. Hench, J. Non-Cryst. Solids, 292 (2001) 115.
17 Z. Strnad, Biomaterials, 13 (1992) 317.
18 Z. Strnad and J. Šesták, 'Bio-compatible ceramics' in the Proceedings of the 3rd Inter. Conf. Intelligent Processing and Manufacturing of Materials, (J. Meel, Ed.) Vancouver Univ., p. 123.
19 A. Šimunek, A. Štepánek, V. Zábrodský, Z. Nathanský and Z. Strnad, Quintessenz, 6 (1997) 3.
20 Z. Strnad, J. Strnad, M. Psotová, C. Povýšil and K. Urban, Quintessenz, 7 (1998) 5.

21 K. Urban, Z. Strnad, C. Povýšil and P. Sponer, Acta Chir. Orthop. Traum. Czech. 63 (1998) 16.
22 J. Strnad, A. Helebrant and J. Hamáčková, Glastech. Ber. Glass Sci. Tech., 73C (2000) 262.
23 Z. Strnad, Glass-ceramic materials; Liquid Phase Separation, Nucleation and Crystallization in Glasses, Elsevier, Amsterdam 1986.
24 L. L. Hench, Glastech. Ber. Glass Sci. Tech., 70C (1997) 439.
25 L. L. Hench, J. Biomed Mater. Res., 23 (1989) 685.
26 L. L. Hench and J. K. West, J. Mater. Sci., 29 (1994) 3601.
27 J. Šesták (Ed.), Vitrification, Transformation and Crystallization of Glasses, special issue of Thermochim. Acta, Vol. 280/281, Elsevier, Amsterdam 1996.
28 J. Šesták, in Z. Chvoj, J. Šesták and A. Triska (Eds), Kinetic Phase Diagrams; Non-equilibrium Phase Transformations, Elsevier, Amsterdam 1991.
29 J. Šesták, Glastech. Ber. Glass. Sci. Tech., 70C (1997) 439.
30 J. Šesták, J. Therm. Anal. Cal., 61 (2000) 305.
31 B. Hlaváček, J. Šesták and J. J. Mareš, J. Therm. Anal. Cal., 67 (2002) 239.
32 J. Šesták and Z. Strnad, in Proc. 8th Int. Conf. Reactivity of Solids, Gothenburg, Elsevier, Amsterdam 1976, p. 410.
33 J. Šesták and Z. Strnad, in Proc. Int. Congress Glass '77, CVTS Publ. House, Prague 1977, Vol. 2, p. 249.
34 N. Koga, Z. Strnad and J. Šesták, Thermochim. Acta, 203 (1992) 361.
35 N. Koga and J. Šesták, Biol. Soc. Esp. Ceram. Vidrio, 31 (1992) 185.
36 M. C. Weinberg, Thermochim. Acta, 280/281 (1996) 63.
37 N. Koga, K. Yamaguchi and J. Šesták, J. Therm. Anal. Cal., 56 (1999) 755.
38 M. C. Weinberg, J. Mining Metal. (Bor, Yugoslavia), 35 (1999) 197.
39 N. Koga and J. Šesták, J. Therm. Anal. Cal., 60 (2000) 667.
40 N. Koga and J. Šesták, J. Am. Ceram. Soc., 83 (2000) 1753.
41 I. M. Steevels, Philips Tech. Rundschau, 9/10 (1960) 337.
42 G. W. Toop and C. S. Samis, Trans. Metal. Soc. AIME, 224 (1962) 878.
43 C. R. Masson, Proc. Roy. Soc. A, 287 (1965) 201.
44 C. R. Masson, J. Am. Ceram. Soc., 51 (1968) 34.
45 C. R. Masson, in Proc. Int. Congress Glass '77, CVTS Publ. House, Prague 1977, Vol. 1, p. 1.
46 K. Závěta and J. Šesták, in Proc. Int. Congress Glass '77, CVTS Publ. House, Prague 1977, Vol. 1, p. 399.
47 L. L. Hench, in P. Ducheyne and J. Lemons (Eds), Bioceramics, Vol. 523, Annals of New York Academy of Sciences, New York 1988, p. 54.
48 L. L. Hench, Handbook of Bioactive Ceramics, Vol.1, CRT Press, 1990, p. 7.
49 C. J. B. Fincham and F. D. Richardson, Proc. Roy. Soc., A223 (1954) 40.
50 M. Temkin, Zh. Fiz. Khim, 20 (1946) 105, (in Russian).
51 P. Balta and E. Balta, Introduction to Physical Chemistry of the Vitreous State, Abacus Press, Kent 1976, Chapter 3.
52 Y. Kawamoto and T. Tomozawa, Phys. Chem. Glasses, 22 (1981) 11.
53 H. M. Kim, F. Miyaji, T. Kokubo, C. Ohtsuki and T. Nakamura, J. Am. Ceram. Soc., 78 (1995) 2405.

6237

Journal of Thermal Analysis and Calorimetry, Vol. 76 (2004)

Please, shorten the title

INTERACTION OF ACID AND ALKALI TREATED TITANIUM WITH DYNAMIC SIMULATED BODY ENVIRONMENT
Mimetic material for the bone tissue substitution Part. II

J. Strnad[1*], *J. Protivínský*[2], *D. Mazur*[3], *K. Veltruská*[3], *Z. Strnad*[1], *A. Helebrant*[2] *and J. Šesták*[4]

[1]Laboratory for Glass and Ceramics, Lasak Ltd., Papírenská 25, CZ-16000 Prague 6, Czech Republic
[2]Department of Glass and Ceramics, Institute of Chemical Technology, Technická 5, CZ-16628 Praha 6, Czech Republic
[3]Department of Electronics and Vacuum Physics, Faculty of Mathematics and Physics of Charles University, V. Holešovičkách, CZ-18000 Prague 8, Czech Republic
[4]Institute of Physics, Academy of Sciences, Cukrovarnická 10, CZ-16253 Prague 6, Czech Republic

Abstract

Interaction of acid and acid+alkali treated titanium samples with simulated body fluid was studied. In case of alkali treated titanium, the dynamic arrangement of the test enabled the detection of primary calcium and phosphate ion adsorption from the solution and later apatite crystal growth (XRD). The induction time for crystal growth was 24.2 0.3 h. On acid-only treated titanium no crystal growth was detected. The calcium phosphate adsorption layer formed on the acid treated samples was detectable by XPS only, however it differed from that one formed on the acid+alkali treated samples. The adsorption layer formed on the acid+alkali treated samples contained larger amount of calcium, especially in the shortest exposure times. Charging of the apatite crystallites during the XPS measurement enabled the determination their Ca/P ratio separately from Ca/P ratio of the adsorption layers. XPS and EDS analyses indicated that the spherulitic crystallites consisted of carbonated hydroxyapatite with the Ca/P ratio close to that one of the stoichiometric hydroxyapatite. It is proposed that the adsorption layer formed spontaneously and immediately on the acid+alkali treated titanium can provide an ideal interface between the metal implant and the apatite cement line, the first structure formed by osteoblast cells during the formation of the new bone on foreign surfaces.

Keywords: bioactivity, body liquid, calcium phosphate, dental implant, EPS, osseointegration, osteoblast, surface treatment, titanium, XPS

Introduction

Titanium has been the most widely used material for dental implants since the late seventies, when its osseointegrative ability was first discovered and documented [1]. At that time the phenomenon of osseointegration was defined as a formation of an

* Author for the correspondence: E-mail: strnad@lasak.cz

1388–6150/2004/ $ 20.00

Akadémiai Kiadó, Budapest
Kluwer Academic Publishers, Dordrecht

intimate contact of the implant with the bone tissue without intermediate layers on the optical microscopy level. Machined titanium implants were used in the early days; later, implants with surface modifications took over offering more stable and long-term functional interface between the implant and the bone bed. Sand-blasted or titanium plasma sprayed implants showed higher bone-implant contact or removal torque values compared to machined surfaces [2, 3]. Currently, chemical modification of titanium by acid etching is introduced to support and speed-up the healing and the bone formation processes around the implant further [4–8]. The acid etching procedure creates a micro-rough texture that is able to retain the fibrin network of the blood clot, through which cells migrate to the surface of the implant where the new bone is formed [8].

Non-metal bioactive materials such as bioactive glasses, glass-ceramic, silica and titania gels or hydroxyapatite have the ability to form a very stable interface with bone tissue by a formation of a calcium phosphate layer on their surfaces as a consequence of chemical interaction with body fluids [9]. The mechanical strength of this interface usually exceeds the strength of the bone tissue to which bioactive material is bonded [10, 11]. Due to their poor mechanical properties, which disable them from application under load-bearing conditions, bioactive materials (especially hydroxyapatite) are applied onto the surface of titanium implants to achieve faster and more reliable bonding with bone tissue. In spite of the success in accelerating the bone healing process and in the increase of the bone-implant contact in the early phases of healing [12–14], hydroxyapatite plasma sprayed coatings were subject to many controversies regarding their long-term stability.

The ability of bioactive materials to form a bone-like apatite on their surfaces in the body can be reproduced in vitro using a simulated body fluid (SBF) [15]. All bioactive materials, e.g. bioactive glasses, glass-ceramics, SiO_2 and TiO_2 gels, use their hydrated surfaces rich in hydroxyl group to adsorb calcium and phosphate ions and induce spontaneous apatite crystal growth within hours or days [9, 16, 17]. It is the kinetic of precipitation that differs from one material to another [18] and it has been shown that the rate of apatite formation is related to the bone bonding ability of material. The most bioactive of contemporary materials – the 45S5 Bioglass® – forms an interfacial apatite layer 0.8 m thick within 1 h of implantation in a rat bone [19].

In contrast to bioactive materials, machined titanium forms calcium phosphate layers in SBF's at much lower rate and the thickness of the precipitated layers is much smaller. Hanawa [20] used XPS to detect apatite-like calcium phosphate layers after immersing c.p. titanium in Hanks balanced salt solution and after 30 days of soaking the thickness of the adsorbed layer was 7.9 nm. Ducheyne [21] detected a calcium phosphate precipitated on the surface of c.p. titanium by XPS only after 30 days of soaking in SBF. It is assumed that c.p. titanium does not provide such suitable surface for apatite formation as bioactive materials and that this can be the cause of its poorer bone-bonding ability (e.g. compared to hydroxyapatite) especially in shorter healing periods and under non ideal healing conditions [14, 22, 23].

Therefore, various attempts have been made to modify the surface of titanium in order to make it bioactive, but without the use of a thick coating of other bioactive material. The most successful methods of titanium bioactivation are e.g. alkali or fluoride treat-

ment [24]. Especially the ability of alkali-treated titanium to induce apatite precipitation after such short times as 24 h of soaking in SBF was well documented [25, 26].

Surface treatments modifying micro-roughness (acid etching) or bioactivity (alkali etching) showed promising results in tests run in-vivo, as well as superior clinical performance compared to machined or grit blasted surfaces [5–7, 27, 28]. It was found that the combination of treatments, ensuring both optimal roughness and bioactive properties, could result in an implant surface with outstanding ability of quick and reliable osseointegration [29]. It was confirmed that acid+alkali treated titanium surfaces induce reproducible apatite formation in vitro [30] and exhibit promising clinical performance [31].

The ion exchange between the biomaterial's surface and the body fluid is the fastest interaction mode; it precedes and affects the adsorption of larger molecules such as amino acids and proteins. Therefore, a hypothesis can be made that the ion exchange has a profound effect on the later stages of the healing process.

The aim of this study was to compare the initial ion interactions of acid and acid+alkali treated titanium with simulated body fluid (SBF) and to discuss the possible effect of the surface treatments on implant healing.

Materials and methods

Preparation of samples

Titanium samples were used in the form of turnings or titanium discs (diameter 14 mm c.p. Ti grade 4), Fig 1. The machined samples (Ti-M) were washed in isopropanol in an ultrasonic cleaner and dried at 110°C. The first group of samples was acid-etched (Ti-AE) in a solution of hydrochloric acid (40°C, 90 min), washed in deionized (DI) water and ethanol in an ultrasonic cleaner. The second group of samples, designated Ti-AAE in

Fig. 1 Samples - titanium discs and turnings used for exposure in SBF

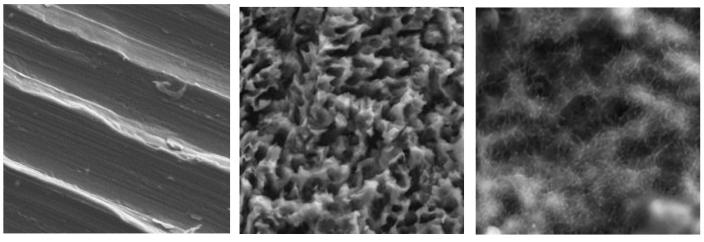

Fig. 2 Surface topography of machined- Ti-M a – acid etched-Ti-AE b – acid and alkali treated – titanium Ti-AAE and c – (SEM, magnification 4000)

this text, was acid-etched under the same conditions and subsequently etched in sodium hydroxide solution (60°C, 4 h), washed in DI water and ethanol in ultrasonic cleaner. All samples were dried at 110°C after washing. The surface topography is showed in Fig. 2.

Experimental arrangement

The SBF solution was prepared using following reagents: KCl, NaCl, $NaHCO_3$, $MgSO_4$ $7H_2O$, $CaCl_2$, Tris, NaN_3 and KH_2PO_4. Tris buffer was used to adjust the pH to 7.55–7.60 at 25°C. Sodium azide was added to inhibit bacterial growth. Samples were exposed in a flow-through reaction cell with SBF preheated at 37°C (Fig. 3). The flow rate of SBF solution through the cell was 0.042 mL min^{-1}. Samples of the output solution were collected for calcium and phosphate ion concentration measurement (Fig. 4). The composition of SBF in comparison to the inorganic part of the blood plasma is given in Table 1. The preparation of the solution was carried out after Jonasova *et al*. [32].

The exposure in SBF is usually carried out as a static experiment, where a sample is placed in the SBF solution of a constant volume, or the solution is periodically renewed [14, 21, 33]. If the solution volume is sufficiently high to keep approximately constant solution composition it is difficult to detect compositional changes in the solution caused by the material-SBF interaction. If the volume is small, concentration changes are measurable but in case of apatite formation the driving force for nucleation and crystallization decreases as calcium and phosphate ions are consumed from the solution. Static exposure

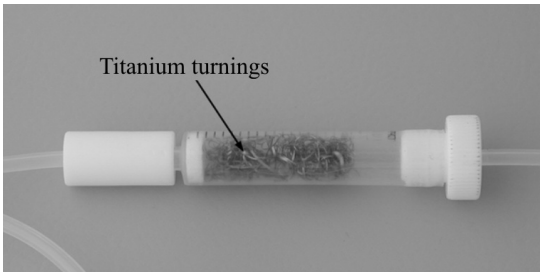

Fig. 3 Flow-through cell used for exposure of samples to SBF

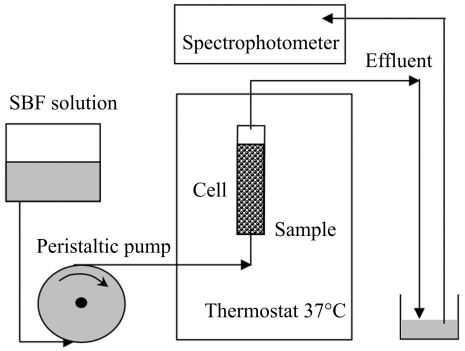

Fig. 4 Experimental arrangement of the exposure in SBF

Table 1 The composition of SBF used in experiments compared to that of human blood plasma

	SBF/mmol L^{-1}	Blood plasma/mmol L^{-1}
Na^+	142.0	137–147.0
K^+	5.0	3.8–5.1
Ca^{2+}	2.5	2.25–2.75
Mg^{2+}	1.0	0.75–1.25
Cl^-	131.0	98–106
HCO_3^-	5.0	24–35
HPO_4^{2-}	1.0	0.65–1.62
SO_4^{2-}	0.5	0.5

also does not resemble the conditions during implantation, where blood circulates. Therefore, a dynamic exposure is suggested to keep constant composition during the experiment and to detect compositional changes in SBF during the initial stages of interaction.

Surface and solution analysis

Composition of the Ti samples' surfaces was analyzed using X-ray photoelectron spectroscopy. UHV facility with Microtech X-ray source and Omicron multi-channel hemispherical analyzer EA 125 was used. The source has Mg/Al dual anode and the Mg anode was used for the measurements. The X-rays were not monochromated. The photoelectron spectra were measured with the analyzer pass energy of 20 eV. The spectra were fitted using a standard fitting procedure with Gaussian–Lorentzian curves.

After exposure in SBF the surface of samples was analyzed by Scanning electron microscopy and energy dispersive spectroscopy (SEM-EDS, Jeol XA-733-superprobe, Jeol USA, Inc.). The EDS analysis results are based on semi-quantitative analysis without the use of standards. X-ray diffraction (XRD) measurements were performed using 3000P diffractometer, Cu anode, measured at 40 kV, 30 mA (Seifert Co., Ahrensburg, Germany).

The concentration of calcium in the output solution was determined using atomic absorption spectroscopy (Varian-Spectr AA300) and phosphate concentration was determined spectrophotometrically (UV-1201, Shimadzu Europe, Ltd.).

The rate of hydration of the prepared titanium samples was measured using FTIR (Fourier transformed infra-red) spectroscopy (Nicolet 740, Nicolet Madison, USA). A wavenumber interval of 400–4000 cm^{-1} was used. Incident radiation angle was 45°.

Results and discussion

Which figure do you mean? Please, refer to figures in order

Concentration changes in the output solution

The time dependence of Ca^{2+} and PO_4^{3-} ion concentration in the output solution, measured after exposure of Ti-AAE samples in SBF, indicated three main phases of interaction **(Fig.)**??. First, a rapid but temporary decrease of calcium and phosphate con-

centration in the effluent was detected. This decrease indicated a significant adsorption of Ca^{2+} and PO_4^{3-} ions by the material. During the second phase, effluent concentration almost returned to its initial value (100 mg L^{-1} Ca^{2+}, 96 mg L^{-1} PO_4^{3-}). Approximately 25 h from the beginning of the experiment, another concentration decrease was detected. This concentration decrease stabilized at the level of 60–63 mg L^{-1} of PO_4^{3-}, indicating the crystal growth at a constant rate. The formation of apatite crystals on the surface of Ti-AAE samples was also confirmed by SEM and XRD measurement **(Fig. 8)**??.

The dynamic experimental arrangement enabled simple determination of the induction times using a plot of total mass of PO_4^{3-} consumed by samples' surfaces *vs*. time and by extrapolation of its late-time linear part to the zero mass (**Fig. 6**). After the induction period, a spontaneous consumption of calcium and phosphate ions from the solution occurred. The induction time value, which is 24.2 0.3 h, is in good agreement with the results obtained using static exposure and reported earlier [26, 34]. In case of Ti-AAE samples the initial calcium and phosphate adsorption was remarkable in the time dependence of the output ion concentrations. The amount of calcium and phosphate ions adsorbed was significantly higher than in case of Ti-AE samples, where no changes in the effluent concentration were detected (Fig. 5).

The finding that only Ti-AAE samples induce apatite formation is in agreement with results of Nancollas *et al*. [35], who detected apatite growth only on the KOH treated titanium surface, whereas on acid (HNO_3) treated titanium the growth did not occur within 3 days of exposure.

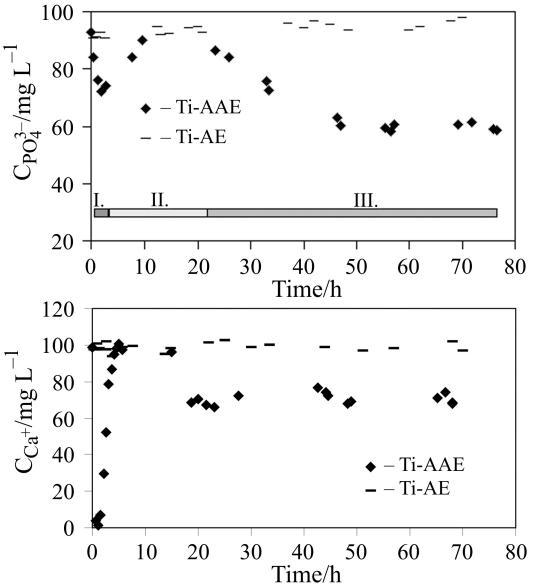

Fig. 5 Time dependence of the PO_4^{3-} and Ca^{2+} concentration in the output SBF solution during exposure of Ti-AE (upper) and Ti-AAE (below) samples, indicating three phases of interaction

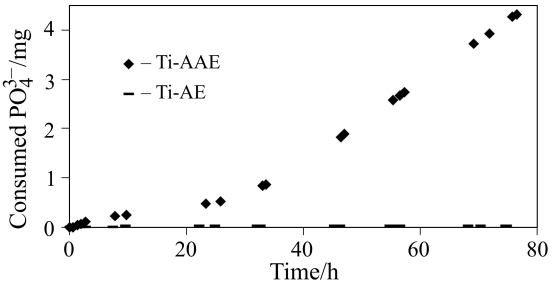

Fig. 6 Time dependence of the precipitated PO_4^{3-} mass plotted for Ti-AAE and Ti-AE samples

FTIR analysis

It was found by Li [16] that not only the negative charge of hydroxyl groups (of titanium oxides) but also their high density on the surface is necessary prerequisite for apatite formation. The FTIR analysis was used to determine the level of hydration of the titanium samples. The peak intensity of hydroxyl groups in the wavenumber range of 3300–3600 was evaluated. The Ti-AAE samples showed significantly higher absorption at 3384.50 cm^{-1} (1.36 Kubelka–Munk units, Fig. 7) compared to Ti-AE samples. The absorption of the Ti-M samples was negligible compared to Ti-AAE. The position of the peak is characteristic to OH groups present e.g. in sol–gel prepared TiO_2 films [36].

These results indicate that the ability of alkali-treated titanium to induce apatite formation can be caused by higher density of hydroxyl groups present in its porous gel-like structure compared to the lower density on the acid-treatedtitanium.

The results of the dynamic flow-through test (Fig. 5) and XPS analysis (Fig. 9) indicate that although ion adsorption occurs on both acid and alkali treated titanium

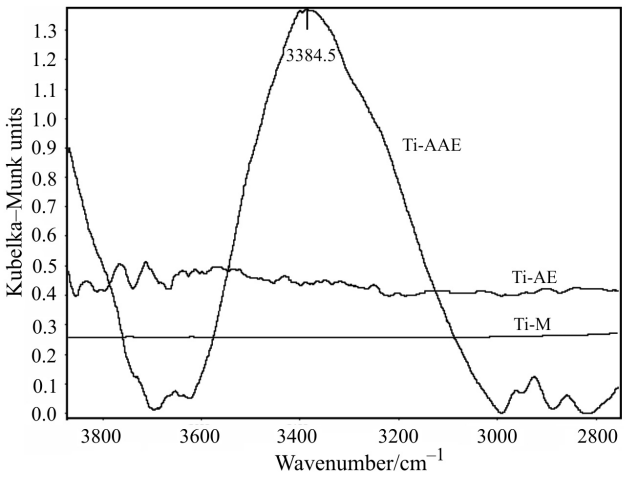

Fig. 7 The FTIR spectrum of Ti-M, Ti-AE and Ti-AAE samples

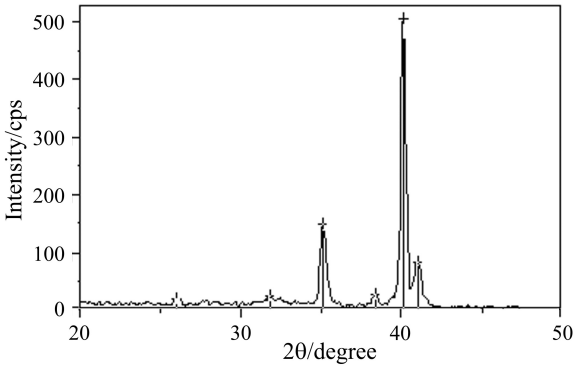

Fig. 8 XRD spectrum of the Ti-AAE sample after 48 h of exposure in SBF solution

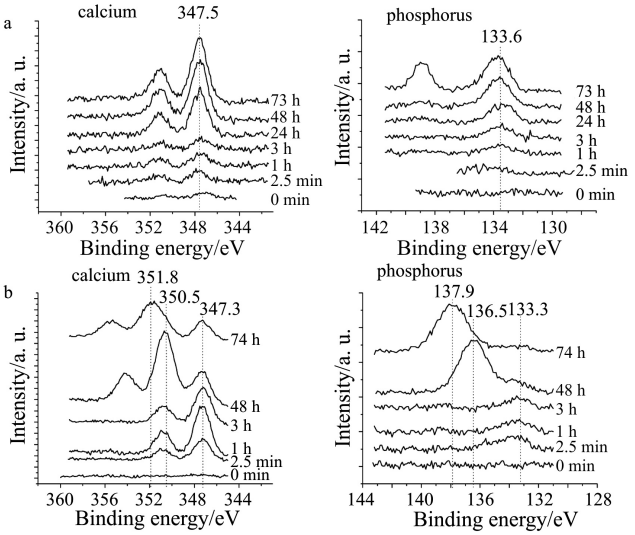

Fig. 9 Photoelectron spectra of Ca 2p and P 2p of a – Ti-AE (HCl-corroded) samples b – Ti-AAE (HCl+NaOH-treated) samples and c – immersed in SBF for various periods of time

surfaces, the adsorbed amount of phosphate and especially calcium ions is larger in case of more hydrated alkali-treated titanium in the first stages of interaction. This could be caused by the detected difference in the density of hydroxyl groups present on the surface of Ti-AAE and Ti-AE samples. It was shown that during the process of peri-implant healing, calcium phosphate cement line containing non-collagenous proteins is formed on the implant's surface before collagenous matrix formation occurs [37, 38].

Intensive calcium adsorption mediated by hydroxyl groups can induce apatite crystal growth but also attract non-collagenous proteins as good calcium binders [39]. By this mechanism an apatite-protein cement layer can be formed on the surface of an implant. Chemical and structural similarity between the preformed cement layer on the

implant's surface and that one produced later by cells can result in a faster formation of a more mechanically stable interface with newly formed bone tissue.

XRD analysis

Although apatite crystallites did not cover the surface of Ti-AAE samples completely, it was possible to detect weak diffraction peaks confirming the presence of hydroxyapatite crystalline phase (Fig. 8).

XPS analysis

On the sample Ti-AE (corroded in HCl without subsequent SBF treatment) carbon C, nitrogen N, oxygen O and titanium Ti were detected, sodium Na was present in barely detectable amount. In the spectrum of Ti-AAE sample (before SBF treatment) sodium Na 1s signal was more intense (by ~3 orders of magnitude) than for Ti-AE sample, as a result of the NaOH treatment. The energetic intervals measured in the photoelectron spectra were those of C 1s, N 1s, O 1s, Na 1s, Ti 2p, Ca 2p and P 2p. In this work, the evolution of calcium and phosphorus spectra was crucial and it will be discussed in detail.

The spectra of carbon, oxygen, calcium and phosphorus exhibited substantially different behavior in case of Ti-AAE compared to Ti-AE samples. In this article, the Ca 2p and P 2p spectra (Fig. 9) are used for illustration. Spectra of O 1s and C 1s evolved likely and they are not shown here. The spectra of Ti 2p showed no difference (between Ti-AE and Ti-AAE samples) and no evolution in peak positions, as well as the N 1s spectra. The intensity of Na 1s peak in Ti-AAE measurements decreased with time in SBF in agreement with models of Kim *et al*. [40] and de Andrade *et al*. [41], for Ti-AE it remained at the just detectable intensity mentioned above. All the analyzed spectra, including those in Fig. 9, were corrected with respect to position of C 1s peak at 285.0 eV to eliminate the shifts in peak positions due to surface charging under X-ray illumination. As shown in Fig. 9, the calcium peak position in case of Ti-AE samples is 347.5 eV, whereas in case of Ti-AAE samples it is 347.3 eV. Additionally, the spectra of Ca 2p of Ti-AAE samples divide in two overlapping peak doublets for the 48 and 74 h periods of SBF treatment. The non-shifted Ca 2p position at 347.3 eV (Ti-AAE samples) corresponds to that of hydroxyapatite [42].

Phosphorus spectra exhibit a similar behavior. For Ti-AE samples, the P 2p peak position is 133.6 eV and it does not change with time of SBF treatment (peak at 138.7 eV shall be discussed later). In case of Ti-AAE samples, the P 2p peak is at 133.3 eV with additional peaks at 136.5 and 137.9 eV, appearing at 48 and 74 h in SBF, respectively. The non-shifted P 2p position at 133.3 eV (Ti-AAE samples) corresponds to that of hydroxyapatite [43].

As shown in Fig. 9, additional intense peaks appeared in calcium and phosphorus spectra of Ti-AAE samples treated in SBF for 48 and 74 h periods. These new peaks are shifted by 3.2 and 4.5 eV, respectively. Similar new peaks at the same shifts from basic positions were observed in the C 1s and O 1s spectra (not shown here),

too. In coherence with SEM observation of crystal growth on the Ti-AAE samples (48 and 74 h of SBF treatment, see SEM-EDS results below) we conclude that the shifted signal comes from the crystallites. The constitution of calcium, phosphorus, oxygen and carbon indicates a carbonated calcium-phosphate nature of the crystallites. Being of insulating nature, the crystallites take on electrical charge. Since they charged independently from the sample surface, i.e. much more, it was possible to distinguish them from the adsorbed calcium- and phosphate-rich layer. The large shift may also indicate their weak bond to the sample surface. The peak at 138.7 eV in P 2p (74 h of SBF treatment) spectrum stands out of all other data, because no spectrum of other elements has shown such a feature. Having eliminated the possibility of presence of foreign element as an impurity on the sample, it was suggested that some phosphorus-based clusters may have formed on the surface. However, another experiment will have to be done to verify this suggestion.

The Ca/P ratios measured for Ti-AE samples and Ti-AAE samples are shown in Fig. 10. Supposing that all 'charged' signal comes from HA crystallites, the Ca/P ratios for the crystallites and for the adsorbed calcium phosphate were calculated separately. For the Ti-AAE samples the Ca/P ratio of the adsorbed layer varies from 2.5 up to 6.2. The Ca/P ratio of the crystallites is in the range from 1.0 to 1.7, that is, significantly lower than the Ca/P ratio of the adsorbed layer. This relation between Ca/P ratios of the adsorbed layer and the growing crystallites corresponds to the model of Takadama *et al*. [43] saying that the calcium deposition precedes the deposition of phosphate groups. The values of Ca/P ratio for the set of Ti-AE samples were between 0.7 and 1.4, which is lower than any of the previous.

From the calcium and phosphorus photoelectron peak positions, as well as from the Ca/P ratio measurements, it can be concluded, that crystallites appearing at Ti-AAE (HCl+NaOH-treated) surfaces consist of carbonated hydroxyapatite. The adsorbed precursor layer created on the surface within the first 24 h could be distinguished from the hydroxyapatite crystallites on basis of the Ca/P ratio, under the as-

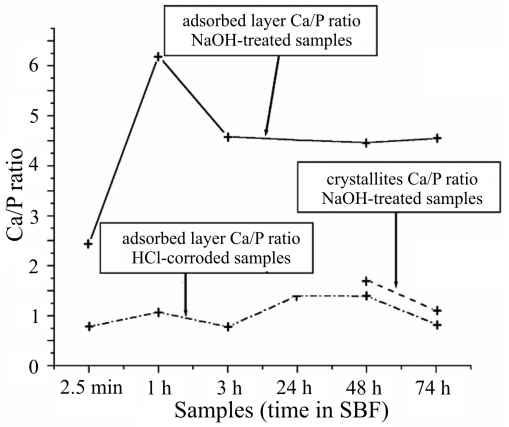

Fig. 10 The Ca/P ratios measured for the Ti-AE (HCl-corroded) samples and Ti-AAE (HCl+NaOH-treated) samples, immersed in SBF for various periods of time

sumption of crystallites charging independently on the adsorbed precursor layer. Between these two no significant difference in binding energies of elements involved has been observed. On the samples with sole HCl treatment (Ti-AE samples), a thin layer of a calcium phosphate (not detected by other methods used), which differs from HA, is created. The Ca/P ratio here is remarkably lower than the Ca/P ratio of the layer adsorbed on NaOH treated (Ti-AAE) samples and the binding energies peak positions differ from those of HA, as discussed above. The primary calcium- and phosphate-rich layers adsorbed on surfaces of Ti-AE and Ti-AAE samples could not be assigned more specific chemical formulae at a reasonable level of confidence. It is a consequence of complicated surface morphology, as well as the fact that XPS spectra of several representatives from the calcium-phosphates family differ too little to distinguish in our measurements [42]. The atomic Ca/P ratio of the crystallites, the coherence in shifts in Ca 2p, P 2p, C 1s and O 1s spectra (48 and 74 h in SBF), and the Ca 2p and P 2p peak positions lead us to a conclusion that the calcium-phosphate developed to the crystals on the Ti-AAE surfaces is most likely carbonated hydroxyapatite. From the Ca/P ratios and SEM observation we conclude that the higher relative abundance of calcium atoms in the adsorbed precursor layer is essential for later formation of hydroxyapatite crystallites.

SEM-EDS

SEM-EDS method was used to detect the changes in the surface structure during exposure in SBF and to analyze precipitates formed on the surface of samples. Figure 11 shows the porous structure of the Ti-AAE samples after exposure in SBF. It can be seen that after 2.5 min up to 24 h only small denser (lighter) areas are formed. These can represent possible nucleation sites of future apatite crystal

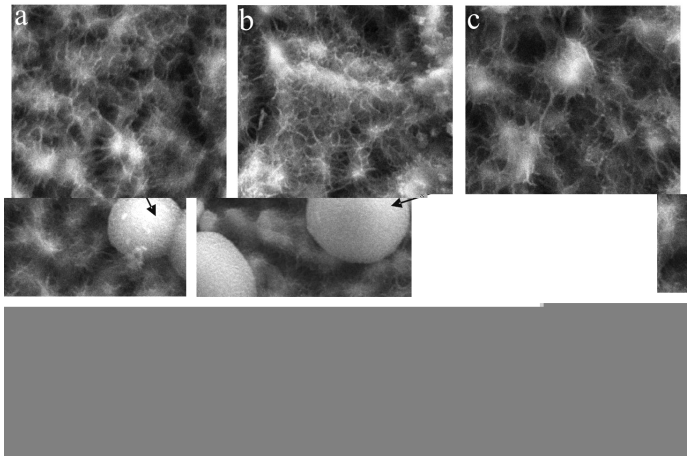

Fig. 11 The surface structure of the Ti-AAE samples after exposure in SBF for a – 2.5 min and b – 1 h c – 24 h d – 48 h e – 72 h (SEM, mag. 4000) (arrows mark the apatite crystallites)

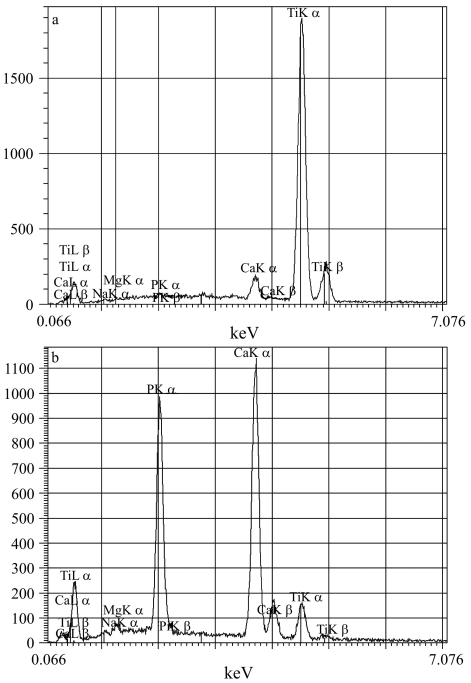

Fig. 12 EDS analysis of the a – crystallite b – the substrate of the sample not covered by the crystallites after exposure of Ti-AAE sample in SBF for 48 h

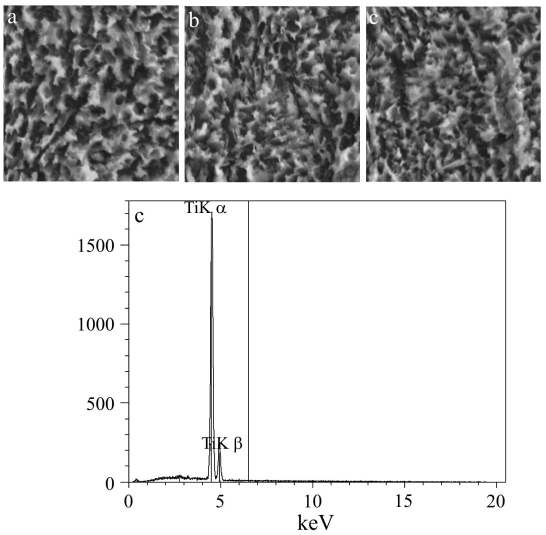

Fig. 13 Surface of the Ti-AE samples after a – 24, b – 48 and c – 72 h of soaking in SBF together with EDS analysis (below) after 48 h of soaking in SBF (SEM-EDS, magn. 4000)

growth. On the sample exposed in SBF for 48 and 72 h formation of crystallites was observed. The SEM-EDS analysis of the Ti-AAE sample exposed in SBF for 48 h is shown in Fig. 12. The analysis indicates that the surface of Ti-AAE sample (not covered by the precipitating crystallites) after exposure in SBF contains a detectable amount of calcium but not detectable (by EDS) amount of phosphorus. The EDS analysis from the spherical crystallite (Fig. 12b) shows strong lines of calcium and phosphorus in the atomic ratio of 1.77, which is slightly higher than that one of stoichiometric hydroxyapatite (1.67). From EDS and XPS results we conclude that spherical bodies consist of hydroxyapatite.

The Ti-AE samples did not show any difference in surface structure and EDS analysis during the exposure in SBF and only titanium was detected after 48 h in SBF (Fig. 13).

Conclusions

The solution analysis during the dynamic SBF test detected calcium and phosphate ionadsorption on the acid+alkali-etched samples in the first stages of interaction. This method was not sensitive enough to detect less intense adsorption in case of Ti-AE samples, where the adsorption layer was detected by XPS analysis. Already after the shortest exposure time of 2.5 min the adsorption layer on the acid+alkali treated samples contained larger amounts of phosphate and especially calcium (also Ca/P ratio was significantly higher than in the case of acid-treated samples). After the induction time of 24.2 h the acid+alkali treated titanium induced apatite crystal growth. The onset of the crystal growth was clearly indicated by the solution analysis.

Charging of the spherulitic crystallites during the XPS measurements allowed us to determine the Ca/P ratio separately for the adsorption layer and the crystallites. Using XPS and EDS analysis the crystallites were identified as carbonated apatite with the Ca/P ratio close to that of stoichiometric apatite. The determination of the induction time could serve as a measure of a substrate ability to support apatite nucleation and growth. The alkali-treated titanium compared to the acid-treated one induced apatite formation in vitro and could therefore provide a suitable substrate for apatite like calcium phosphate precipitates in the cement lines formed on the implants surfaces during the process of new bone formation.

The study is continuation of the series of our communication dealing with glass-ceramic substance and surfaces [44, 45] perspective as mimetic materials for the bone tissue substitution particularly applicable in the dental practice.

This study was supported by the Ministry of Industry and Trade of Czech Republic under the project number FB-CV/64 as well as by the Grant Agency of Academy of Sciences of Czech Republic under the project number A 4010101 and was also a part of the research program MŠMT 113200002 financed by the Ministry of Education of Czech Republic.

References

1 P. I. Brånemark, Scand. J. Plast. Reconstr. Surg., 3 (1969) 81.
2 A. Wennerberg, T. Albrektsson, C. Johansson and B. Andersson, Biomaterials, 17 (1996) 15.
3 K. Gotfredsen, T. Berglundh and J. Lindhe, Clin. Implant. Dent. Relat. Res., 2 (2000) 120.
4 M. Roccuzzo, M. Bunino, F. Prioglio and S. D. Bianchi, Clin. Oral Implants Res., 12 (2001) 572.
5 D. L. Cochran, D. Buser, C. M. Bruggenkate, D. Weingart, T. M. Taylor, J. P. Bernard, F. Peters and J. P. Simpson, Clin. Oral Implants Res., 13 (2002) 144.
6 P. R. Klokkevold, P. Johnson, S. Dadgostari, A. Caputo, J. E. Davies and R. D. Nishimura, Clin. Oral Implants Res., 12 (2001) 350.
7 W. Khang, S. Feldman, C. E. Hawley and J. Gunsolley, J. Periodontol, 72 (2001) 1384.
8 R. J. Lazzara, Bone response to Dual Acid-Etched and Machined Titanium Implant Surfaces. In: J. E. Davies (Ed.) 'Bone engineering' Toronto, Em squared Inc 2000, p. 381.
9 T. Yamamuro, L. L. Hench and J. Wilson, Handbook of Bioactive Ceramics, CRC Press 1990.
10 T. Kokubo, S. Ito, M. Shigematsu, S. Sakka and T. Yamamuro, J. Mater. Sci., 22 (1987) 4067.
11 U. Gross, R. Kinne, H. J. Schmitz and V. Strunz, CRC Critical Reviews in Biocompatibility, 4 (1988) 2.
12 S. Vercaigne, J. G. Wolke, I. Naert and J. A. Jansen, Oral. Implants Res., 9 (1998) 261.
13 L. Sun, C. C. Berndt, K. A. Gross and A. Kucuk, J. Biomed. Mater. Res., 58 (2001) 570.
14 Z. Strnad, J. Strnad, C. Povýšil and K. Urban, J. Oral and Maxillofacial Implants, 15 (2000) 483.
15 T. Kokubo, H. Kushitani, S. Sakka, T. Kitsugi and T. Yamamuro, Mater. Res., 24 (1990) 721.
16 P. Li, C. Ohtsuki, T. Kokubo, K. Nakanishi, N. Soga and K. de Groot, J. Biomed. Mater. Res., 28 (1994) 7.
17 P. Li, X. Ye, I. Kangasniemi, J. M. de Blieck-Hogervorst, C. P. Klein and K. de Groot, J. Biomed. Mater. Res., 29 (1995) 325.
18 L. L. Hench, Surface reaction Kinetics and Adsorption of biological moieties: A mechanistic Approach to tissue Attachment. In J. E. Davies (Ed.), Bone engineering, Toronto, Em. squared Inc. 2000, p. 381.
19 L. L. Hench and O. Andersson, Bioactive glasses. In: L. L. Hench, J. Wilson (Eds) 'An introduction to bioceramics', Florida, World Scientific Publishing 1993, p. 41.
20 T. Hanawa, Titanium and its oxide film: A substrate for formation of apatite. In: J. E. Davies (Ed.) Bone-biomaterial interface, Toronto, Em squared Inc. 2000, p. 49.
21 P. Li and P. Ducheyne, J. Biomed. Mater. Res., 41 (1998) 341.
22 K. Soballe, Acta Orthop. Scand. Suppl., 255 (1993) 1.
23 K. Soballe, E. S. Hansen, H. Brockstedt-Rasmussen, V. E. Hjortdal, G. I. Juhl, C. M. Pedersen, I. Hvid and C. Bunger, Clin. Orthop., 272 (1991) 300.
24 J. E. Elingsen, On the properties of surface-modified titanium. In: J. E. Davies, (Ed.) Bone engineering, Toronto, Em squared Inc. 2000, p. 183.
25 H. M. Kim, F. Miyaji and T. Kokubo, J. Mater. Sci.: Mater. in Medicine, 8 (1997) 341.
26 H. M. Kim, F. Miyaji, T. Kokubo, S. Nishiguchi and T. Nakamura, J. Biomed. Mater. Res., 45 (1999) 100.
27 T. Kokubo, H. M. Kim, S. Nishiguchi and T. Nakamura, In vivo formation induced on titanium metal and its alloys by chemical treatment in Bioceramics. In: Proceedings of the 13th Int. Symp. on Ceramics in Medicine, Bologna, Italy, Trans. Tech. 2001, p. 3.

28 S. Nishiguchi, T. Nakamura, M. Kobayashi, W. O. Yan, H. M. Kim, F. Miyaji and T. Kokubo, The effect of heat treatment on bone bonding ability of alkali-treated titanium. In: Bioceramics, Vol. 10, Proceedings of the 10th Int. Symp. on Ceramics in Medicine, Paris, France, Elsevier 1997, p. 561.
29 A. Šimůnek, J. Strnad, J. Novák, Z. Strnad, D. Kopecká and R. Mounajjed, Clin. Oral. Impl. Res., 12 (2001) 393.
30 L. Jonášová and J. Hlaváč, Effect of chemical treatment of titanium on apatite formation. In: H. Stallforth and P. Revell (Eds) 'Materials for medical engineering', Euromat 99, Weinheim, Wiley-VCH 2000, p. 126.
31 A. Šimůnek, J. Strnad and A. Štěpánek, Clin. Oral Impl. Res., 13 (2002) 4.
32 A. Helebrant, L. Jonášová and L. Šanda, Ceramics/Silikáty (Prague), 46 (2002) 9.
33 K. Hata, T. Kokubo, T. Nakamura and T. Yamamuro, J. Am. Ceram. Soc., 78 (1995) 1049.
34 J. Strnad, A. Helebrant and J. Hamáčková, Glastech. Ber. Glass. Sci. Technol., 73 (2000) C1.
35 G. H. Nancollas and W. Wu, The controlled nucleation and growth of selected calcium phosphate phases on modified titanium implant surfaces. In: Proceedings of Sixth World Biomaterial Congress, Hawaii: Society for Biomaterials, USA 2000.
36 Y. Djaoued, S. Badilescu, P. V. Ashrit and J. Robichaud, Internat. J. Vibrational Spectroscopy, 5 (2003) 6.
37 J. E. Davies and N. Baldan, J. Biomed. Mater. Res., 36 (1997) 429.
38 M. M. Hosseini, J. Sodek, R. P. Franke and J. E. Davies, The structure and composition of the bone implant interface. In: J. E. Davies (Ed.) Bone engineering, Toronto, Em squared Inc 2000, p. 295.
39 E. D. Eanes, Dynamics of calcium phosphate precipitation. In: E. Bonucci (Ed.), 'Calcification in Biological Systems', Boca Raton, CRC Press 1992, p. 1.
40 H. M. Kim, F. Miyaji, T. Kokubo and T. Nakamura, J. Biomed. Mat. Res., 32 (1996) 409.
41 M. C. de Andrade, M. R. T. Filgueiras and T. Ogasawara, J. Biomed. Mat. Res., 46 (1999) 441.
42 S. Kačiulis, G. Mattogno, L. Pandolfi, M. Cavalli, G. Gnappi and A. Montenero, Appl. Surf. Sci., 151 (1999) 1.
43 H. Takadama, H. M. Kim, T. Kokubo and T. Nakamura, J. Biomed. Mater. Res., 55 (2001) 185.
44 J. Šesták, J. Therm. Anal. Cal., 61 (2000) 305.
45 N. Koga, Z. Strnad, J. Šesták and J. Strnad, J. Therm. Anal. Cal., 71 (2003) 927.